ISSN 2706-655X Vol. 8, Issue 2: 80-93, DOI: 10.25236/IJFET.2026.080211

# Crash Analysis and Structural Optimization of Racing Car Chassis Based on LS-DYNA

**Ting Feng[1], Jing Zhang[2], Yi Hu[2,*]**

[1]*School of Mechatronics Engineering, Wuhan University of Technology, Wuhan, China*
[2]*School of Automotive Engineering, Wuhan University of Technology, Wuhan, China*
**Corresponding author: huyi0820@whut.edu.cn*

***Abstract:*** *This study investigates the crashworthiness and structural optimization of a racing car space-frame chassis under extreme off-road collision conditions. A three-dimensional chassis model was established in CATIA, and a frontal rigid-wall collision at 11.11 m/s was simulated using LS-DYNA. The results show that the chassis undergoes progressive plastic collapse, during which kinetic energy is rapidly converted into structural internal energy. The front longitudinal beams and diagonal braces are identified as the main energy-absorbing components, and deformation propagates from the front structure toward the rear while the occupant cabin remains largely intact. The peak contact force reaches approximately* $1.68\times10^5$ *N, and stress concentration occurs mainly at the welded joints between the front cabin and the driver's cabin. The maximum equivalent stress is about 131 MPa, while the peak plastic strain reaches 0.342, close to the material failure threshold of 0.35, indicating a critical weak region. The front bumper acceleration reaches about 13 g with a steep impact pulse. Based on these findings, local reinforcement and structural simplification were performed to improve safety and reduce mass. After optimization, the maximum plastic strain decreases from 0.342 to 0.148, and the peak front bumper acceleration decreases from 13 g to 8.6 g. The optimized chassis shows improved strain control, smoother energy absorption, and better crashworthiness, providing a useful reference for lightweight design and collision safety improvement of off-road racing car chassis.[1]*

***Keywords:*** *Racing car; Chassis; Collision simulation; LS-DYNA; Structural optimization*

## 1. Introduction

Racing cars are designed to be compact and lightweight, with the objective of achieving superior mobility, durability, and safety across complex and harsh off-road terrains. Under extreme conditions such as high-speed off-road driving, jumps, and sharp turns, racing cars are exposed to significant risks of collision and rollover. Therefore, the chassis, as the primary load-bearing and safety-protective structure of the vehicle, directly affects the driver's safety and the car's ability to complete a race, rendering it a critical subject of study.

Traditional chassis design often relies on engineering experience, static mechanical analysis, and simplified assumptions, which are insufficient to accurately simulate the complex dynamic responses of a vehicle during high-speed collisions, including large deformations, material nonlinearity, contact interactions, and energy absorption. Such limitations may result in overly conservative designs that increase unnecessary weight or introduce latent safety hazards leading to unexpected failures during actual collisions, making dynamic simulation analysis of racing car chassis essential.[2][3][4]

Therefore, addressing collision safety under complex conditions, this study employs LS-DYNA to perform numerical simulations of frontal rigid collisions of the chassis, focusing on deformation patterns, stress-strain distribution, energy conversion characteristics, and dynamic response behaviors during collision. Based on these analyses, weak structural areas are identified, and chassis optimization is performed in line with lightweight design principles. A research workflow of "modeling – simulation – analysis – optimization" is established to provide theoretical and practical guidance for chassis design and safety enhancement.

## 2. Vehicle Optimization Framework Design

In vehicle safety studies, for the typical scenario of a chassis colliding with a rigid wall, the research

ISSN 2706-655X Vol. 8, Issue 2: 80-93, DOI: 10.25236/IJFET.2026.080211

workflow can be systematically divided into several key steps, as illustrated in Figure 1. First, a high-fidelity chassis model is established based on actual structural dimensions and material properties. Second, finite element pre-processing is conducted, including mesh generation, contact definitions, and boundary condition settings, to simulate the collision process between the chassis and the rigid wall. Third, finite element post-processing is performed to extract response parameters such as acceleration, stress, and energy variations. Based on these results, simulation outcomes are evaluated to assess deformation patterns and energy absorption characteristics during collision. Finally, comparative analysis of chassis structures identifies weak points, and optimization is performed based on simulation results, such as modifying cross-sectional shapes, adding reinforcements, or adjusting material distribution, to enhance crashworthiness. This workflow reflects a closed-loop research approach from modeling and simulation to structural optimization, providing theoretical and practical guidance for improving vehicle passive safety.[5]

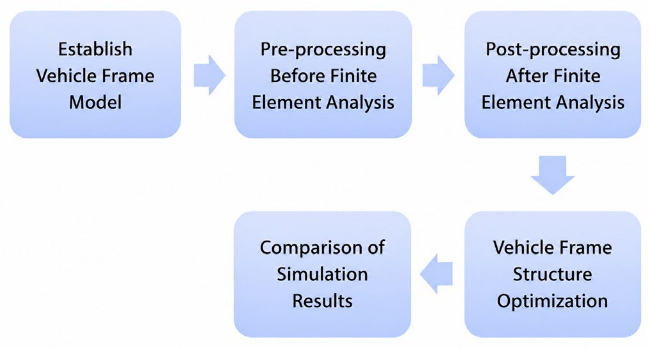


*Figure 1: General Flow Chart of Vehicle Optimization.*

## 3. 3D Chassis Model Construction

The chassis structure used in the simulation has the following characteristics:

1) Regulatory compatibility: the design follows specific roll cage strength standards and driver cabin safety dimension constraints to ensure that key components, such as the main and front rings, meet geometric and material specifications.

2) Structural performance constraints: the chassis must have sufficient strength and stiffness to withstand impact loads during dynamic driving and collision with walls, ensuring the structural integrity of the driver's cabin.

3) Spatial integration constraints: the chassis must have a rational spatial topology layout to accommodate the powertrain, suspension joints, steering mechanism, braking system, and driver anthropomorphic model within a limited size envelope.

The chassis model was constructed using CATIA R20, as shown in Figure 2.

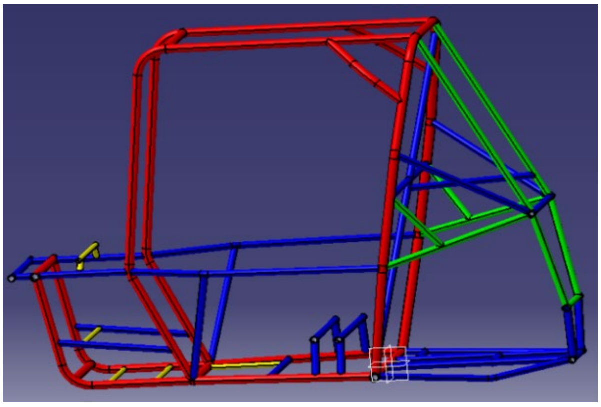

*Figure 2: 3D Vehicle Frame Model.*

This chassis is a typical space-frame structure, divided into the front cabin, driver's cabin, and rear cabin, with the front and driver's cabins integrated in the solid model. The CPQ triangular support in the

ISSN 2706-655X Vol. 8, Issue 2: 80-93, DOI: 10.25236/IJFET.2026.080211

front chassis serves as the boundary between the driver and front cabin.

The red regions represent the main structural components, including the roll cage and triangular supports; the blue regions indicate the front crash structures and suspension mounting points; the green and other blue regions represent the lower and rear structures, including longitudinal and cross beams and rear suspension mounts.

The chassis is constructed from 4130 steel tubes, with outer diameters and wall thickness specifications shown in Table 1.

*Table 1: Component Specifications.*

| | | |
|---|---|---|
| Main Structural Components (Unit: mm) | Red | Φ31.75*1.6 |
| Secondary Component 1 (Unit: mm) | Blue | Φ25*1.7 |
| Secondary Component 2 (Unit: mm) | Green | Φ25*1.3 |
| Secondary Component 3 (Unit: mm) | Yellow | Φ20*1.0 |

## 4. Finite Element Pre-processing

In CAE analysis, the accuracy of the simulation results largely depends on the mesh quality. The chassis main structure is modeled using shell elements, and the mesh is generated in Deviation mode, with a maximum element size of 20 mm, minimum size of 2 mm, a maximum deviation from the original geometry of 0.15, and a maximum allowable angle between adjacent elements of 20°, as shown in Table 2. Quadrilateral shell elements are used for meshing, and mesh quality is rigorously verified using LS-PrePost. The results indicate that quadrilateral elements account for 99.2% of the model, while triangular elements are less than 1%. All elements have a Jacobian determinant ≥0.6, and key metrics such as skewness, warpage, and interior angles meet preset control standards, with 0% invalid elements, ensuring mesh quality suitable for LS-DYNA explicit dynamic simulations in terms of stability and accuracy. Material constitutive modeling adopts the MAT_PIECEWISE_LINEAR_PLASTICITY (MAT_024) model in LS-DYNA, suitable for isotropic elastic-plastic materials in collision simulations. 4130 steel tubes are used, with an elastic modulus of 215 GPa, density of 7850 kg/m³, Poisson's ratio of 0.3, yield strength of 0.785 GPa, and tangent modulus of 2.15 GPa, as shown in Table 3. Based on the initial distance between the chassis and the rigid wall (~0.39 m) and the collision speed (11.11 m/s) along the positive X-axis, the estimated contact time is approximately 35 ms. To fully observe rebound and residual deformation after collision, the simulation termination time is set to 70 ms, and a time scale factor of 0.9 is applied to enhance computational efficiency while maintaining numerical stability.

*Table 2: Mesh Division*

| | |
|---|---|
| Mesh Mode | Deviation |
| Mesh Type | Mixed |
| Max Elem Size | 20 |
| Min Elem Size | 2 |
| Max Deviation | 0.15 |
| Max Angle | 20 |

*Table 3: Material Properties*

| | |
|---|---|
| RO | 7850kg/m³ |
| E | 215GPa |
| PR | 0.3 |
| SIGY | 0.785Gpa |
| ETAN | 2.15 |

*Table 4: Contact Settings*

| Parameter Name | Parameter Value | Description |
|---|---|---|
| SURFA | 2 | Contact surface A ID (frame surface) |
| SURFB | 3 | Contact surface B ID (rigid wall surface) |
| FS | 0.25 | Static friction coefficient |
| FD | 0.25 | Dynamic friction coefficient |
| BT | $1.0\times10^{20}$ | Contact stiffness (penalty stiffness). A very large value simulates rigid contact |
| PENCHK | 0 | Penetration check flag: 0 = off |

ISSN 2706-655X Vol. 8, Issue 2: 80-93, DOI: 10.25236/IJFET.2026.080211

*Table 5: Anti-Penetration Settings*

| Parameter Name | Parameter Value | Description |
|---|---|---|
| SURFA | 2 | Contact surface A ID |
| SURFB | 1 | Contact surface B ID |
| SURFATYP | 3 | Type of contact surface A: 3 indicates slave surface |
| SURFBTYP | 3 | Type of contact surface B: 3 indicates slave surface |
| SAPR | 1 | Contact parameter ID for contact surface A |
| FS | 0.35 | Static friction coefficient |
| FD | 0.25 | Dynamic friction coefficient |
| PENCHK | 1 | Penetration check flag: 1 = enabled |
| DT | $1.0\times10^{20}$ | Contact stiffness (penalty stiffness). A very large value simulates rigid contact |

The contact setup adopts a master-slave contact algorithm, with the rigid wall defined as the master surface and the chassis surface as the slave surface. Both static and dynamic friction coefficients are set to 0.25, and contact stiffness is set to a very high value ($1\times10^{20}$) to simulate near-rigid contact behavior, while penetration checks are disabled to improve computational efficiency.

For internal contacts among chassis components, a symmetric slave-slave contact definition is applied. The static friction coefficient is set to 0.35 and the dynamic coefficient to 0.25, with the higher static friction reflecting the greater tangential force required to overcome initial sliding between metal components. Contact stiffness is similarly set to a high value to ensure the physical accuracy of interactions, and penetration checks are enabled to precisely capture interactions between deformable bodies, preventing simulation distortions due to penetration, as detailed in Tables 4 and 5.

The entire simulation is computed based on the initial distance between the frame and the rigid wall, as well as the initial velocity. The termination time is set to 70 ms, which is considered reasonable. This value is further validated by the simulation results. Additionally, the time scaling factor is set to 0.9.

*Table 6: Equivalent Plastic Strain Failure Threshold*

| Parameter Name | Parameter Value | Description |
|---|---|---|
| MID | 1 | Material ID |
| NUMFIP | 1.0000000 | Number of failure integration points triggering element deletion |
| NCS | 1.0000000 | Number of failure criteria |
| MXEPX | 0.35 | Maximum failure principal strain threshold |
| DMGEXP | 1.0000000 | Damage evolution exponent |

As shown in Table 6, this is a critical part of the pre-processing, defining the equivalent plastic strain threshold for material failure. A value of 0.35 indicates that when the cumulative plastic strain of an element reaches 35%, the element is deleted (failure), simulating material fracture. This directly determines when and where the chassis begins to fail during collision. When using a damage accumulation model, this value influences the damage evolution pattern, with 1.0 typically representing linear accumulation. It also controls the degradation rate of load-bearing capacity after element failure. Post-processing allows observation of which elements fail first, enabling precise identification of the weakest regions in the chassis and providing a direct basis for subsequent structural optimization, such as local reinforcement or modification of tube thickness or material.

## 5. Simulation Results Analysis and Post-processing

### *5.1. Overall Deformation Analysis*

To clearly illustrate the overall deformation of the chassis during the collision, Figures 3(a), (b), (c), and (d) depict the deformation at 33 ms, 38 ms, 43 ms, and 49 ms, respectively. The chassis undergoes a typical dynamic progression from initial contact through energy absorption to full deformation, with deformation exhibiting cumulative and progressive characteristics over time.[6]

At 38 ms (initial deformation stage), compared to 33 ms (initial contact stage), slight overall rearward displacement or compression is observed in the front and middle regions of the chassis. The structural outline remains largely intact, although key members—particularly the front diagonal braces, front bumper, and side crash bars—may have already entered plastic yielding.

ISSN 2706-655X Vol. 8, Issue 2: 80-93, DOI: 10.25236/IJFET.2026.080211

At 43 ms (intensified deformation stage), deformation significantly increases, with the front region of the chassis showing pronounced overall compression and bending, resulting in a reduction of longitudinal length. The geometry of the middle occupant cabin begins to visibly change, indicating that collision energy has been transmitted to the main structure.

At 49 ms (stable/maximum deformation stage), the chassis deformation reaches its peak in this sequence. The front structure collapses further, resulting in a fundamental change in the overall chassis shape compared to the initial state, and the occupant cabin frame may also experience overall bending.

From the images at 43 ms and 49 ms, it can be inferred that the front diagonal braces and longitudinal beams are the primary energy-absorbing components, whose axial compression and bending are the main reasons for the reduction of the overall chassis profile and the collapse of the front geometry.

The energy absorption path is clear: deformation initiates at the foremost part of the chassis and gradually propagates rearward, aligning with the designed energy transfer path. The front structure effectively functions as a "sacrificial zone." Occupant cabin integrity is maintained: although noticeable deformation occurs in the front and adjacent regions, the images indicate that, up to 49 ms, the main frame of the occupant cabin (the primary roll cage structure) remains essentially intact without catastrophic collapse.

Optimization direction: The simulation results clearly identify the front energy-absorbing structure as the critical region for deformation control and energy absorption. Subsequent structural optimization should focus on the cross-sectional dimensions, wall thickness, and material grade of the members in this area, as well as the stiffness and tear resistance of the joints. Through optimization, these components can absorb more energy within controlled deformation while transmitting residual forces smoothly to the robust occupant cabin.

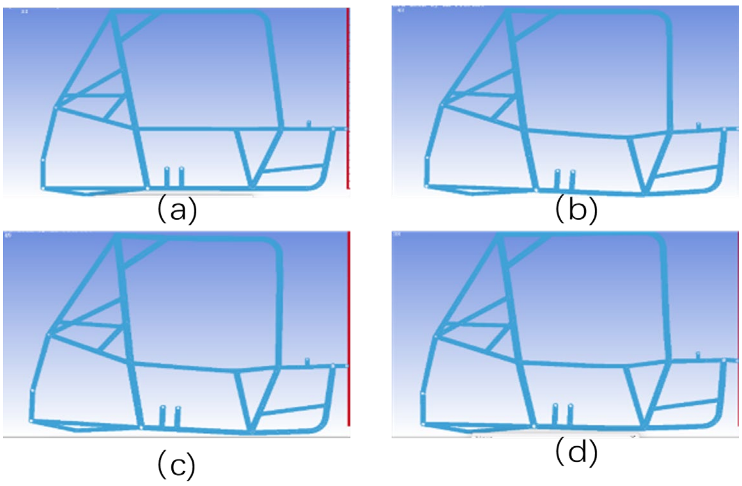


*Figure 3: Deformation characteristics*

### *5.2. Stress and Strain Analysis*

The strain contour plot in Figure 4 shows that the maximum strain concentration occurs at the welded joints during the collision, which is consistent with the expected mechanical response of the structure. The color gradient from blue to orange represents increasing stress or strain levels. The orange regions correspond to high-stress concentration zones or areas of large plastic deformation, which are not only the primary locations for collision energy absorption but also the critical weak points where yielding or initial failure is most likely to occur. Therefore, identifying these regions is the primary objective of structural optimization.

The element history curve in Figure 5 quantifies the damage evolution of a specific high-risk element over time. The curve indicates that the effective plastic strain of this element increases sharply after approximately 30 ms and stabilizes after approximately 40 ms, reaching a peak value of 0.342. This value is very close to the predefined material failure threshold of 0.35, indicating that this location is close to failure under the current design. Overall, the contour plot identifies the structural regions requiring reinforcement, particularly the connection between the front cabin and the driver's cabin where the peak strain approaches 0.342. Targeted reinforcement measures, such as locally increasing wall thickness,

ISSN 2706-655X Vol. 8, Issue 2: 80-93, DOI: 10.25236/IJFET.2026.080211

optimizing geometric configuration, or adopting higher-strength materials, should be considered to ensure that the plastic strain remains sufficiently below the failure threshold during collision, thereby maintaining core safety while pursuing lightweight design. The strain in the rear structure remains below 0.05 throughout the process, indicating good structural integrity.

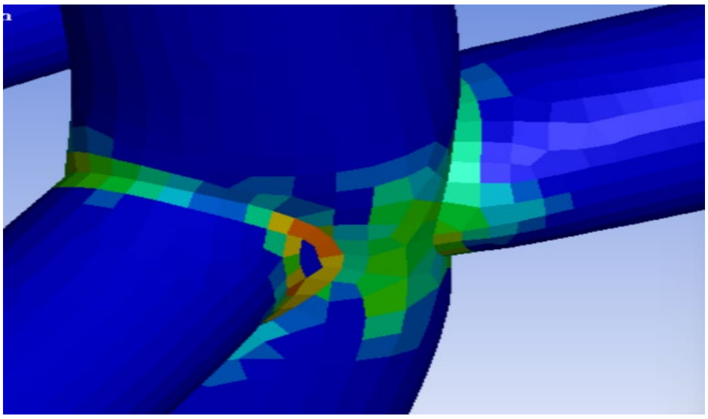

*Figure 4: Strain Contour Plot.*

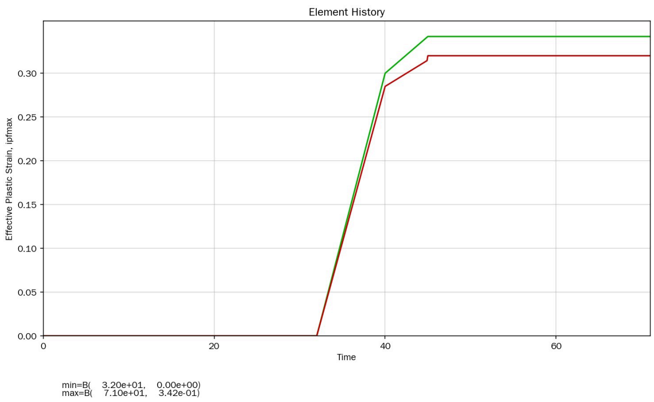


*Figure 5: Time History of Plastic Strain at the Location of Maximum Strain.*

### *5.3. Acceleration Analysis*

The crashworthiness of the chassis is closely related to the acceleration of its center of mass and the amount of energy absorbed. Therefore, collision acceleration is an important indicator for evaluating chassis crashworthiness. During a vehicle collision, energy dissipation is a dynamic process, resulting in continuously varying deceleration throughout the impact event. At the instant of collision, the kinetic energy is almost immediately converted into other forms of energy, and because the collision duration is extremely short, the energy lost through friction is much smaller than the vehicle's kinetic energy. It can therefore be reasonably assumed that nearly all the total energy of the vehicle before impact is absorbed by structural deformation. According to the energy relationship,

$$E=\frac{1}{2}MV_0^2=M\int_0^t a(t)v(t)dt \tag{1}$$

where E denotes the total energy, M denotes the chassis mass, the initial velocity represents the pre-impact velocity of the chassis, a(t) represents chassis acceleration, and v(t) represents the velocity of the chassis center of mass during collision, the energy during the collision process is associated with the acceleration and velocity of the chassis center of mass. Because acceleration varies continuously throughout the collision and the exact position of the center of mass is difficult to determine, this study mainly evaluates the acceleration responses of the front bumper and seat mounting regions as indicators of crash performance. Additional evaluation indicators are also considered. The first is the average acceleration during chassis collision.

$$a=\frac{1}{T}\int_0^t a(t)dt \tag{2}$$

ISSN 2706-655X Vol. 8, Issue 2: 80-93, DOI: 10.25236/IJFET.2026.080211

Based on the relationship between acceleration and impact load, a lower average acceleration corresponds to a lower average load acting on the chassis. The second indicator is the root mean square acceleration during collision.

$$\sigma = \sqrt{\frac{1}{T}\int_0^t (a-a^{0)})^2 dt} \tag{3}$$

A larger deviation between the instantaneous acceleration and the mean acceleration indicates greater acceleration fluctuation and therefore poorer safety performance. The maximum acceleration is also considered, and these three indicators complement one another to provide a more comprehensive evaluation.

All acceleration values presented below are averaged from more than three measurement points. Figure 6 shows the acceleration response of the front bumper during collision, Figure 7 illustrates the acceleration response at the rear part of the seat mounting position, and Figure 8 presents the acceleration response at the front part of the seat mounting position.

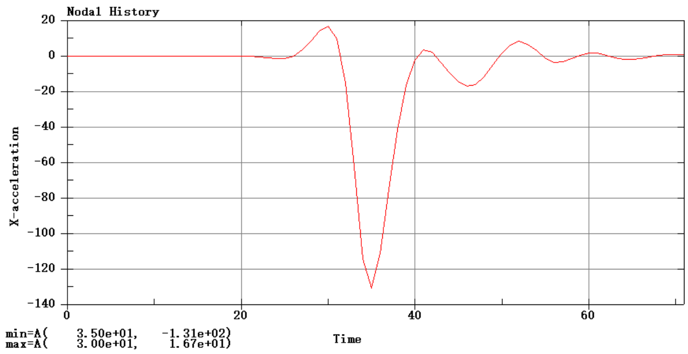


*Figure 6: Average Acceleration of the Front Bumper.*

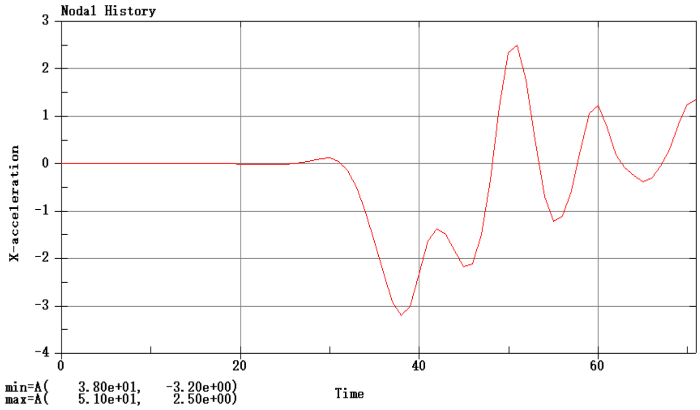


*Figure 7: Average Acceleration at the Rear Seat Mounting Position.*

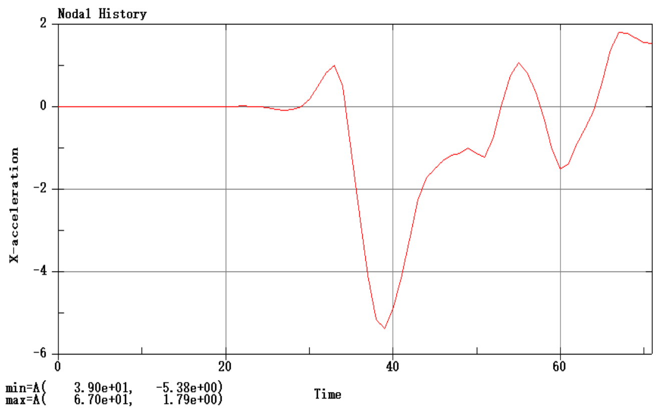


*Figure 8: Average Acceleration at the Front Seat Mounting Position.*

ISSN 2706-655X Vol. 8, Issue 2: 80-93, DOI: 10.25236/IJFET.2026.080211

The acceleration begins to rise sharply at an average time of approximately 29 ms and reaches its peak at around 38 ms, with the peak acceleration of the front bumper reaching 13 g. The rising edge of the impact pulse is extremely steep, with a rise time of only approximately 8 ms, indicating that the load is applied very rapidly during the early collision stage and that the impact severity is relatively high. Regarding data validity, the data used in this analysis were filtered according to SAE J211/ISO 6487 using the CFC 60 channel frequency class, effectively removing high-frequency numerical noise and ensuring the engineering reliability and comparability of the results. A preliminary safety assessment indicates that the current chassis design can establish an effective energy absorption mechanism during collision; however, the impact pulse transmitted to the occupant cabin remains relatively steep and is accompanied by subsequent vibration. The presence of rebound acceleration and the relatively smooth post-impact vibration curve suggest that the plastic deformation structure of the chassis has good energy absorption capacity with a certain safety margin.

Subsequent structural optimization should focus on reducing peak acceleration and smoothing the impact pulse waveform. By refining the design of the front energy-absorbing structure and optimizing the overall load path, the chassis can achieve an integrated improvement in lightweight performance and crashworthiness while ensuring occupant safety. This analysis provides a clear performance benchmark and improvement direction for subsequent optimization iterations.

### *5.4. Energy Analysis*

Vehicle collision is essentially an energy conversion process in which kinetic energy is transformed into internal energy and other forms of energy. The main energy components during the collision include kinetic energy, internal energy, and sliding energy. Their sum constitutes the total energy, which remains constant throughout the collision process.

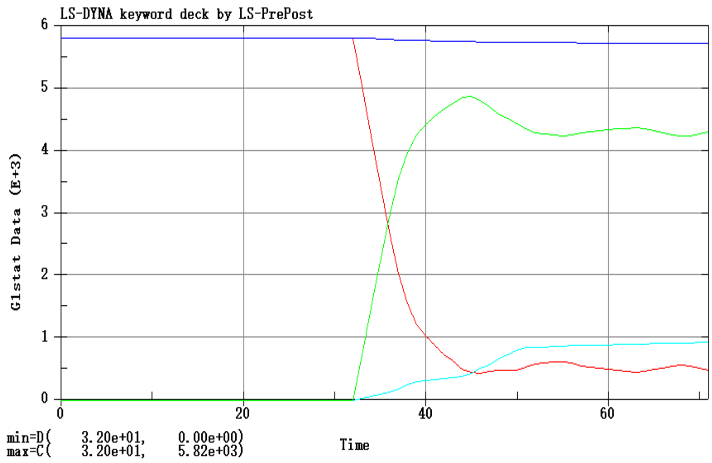


*Figure 9: Energy Variation.*

As shown in Figure 9, the blue curve represents the total energy, which remains nearly horizontal throughout the collision process, indicating that the simulation results are reliable and free from nonphysical energy dissipation or sudden energy growth. The red curve represents kinetic energy, which remains at its maximum value at the initial moment of impact and then rapidly decreases to nearly zero within a very short time, fully consistent with the physical behavior of a rigid barrier collision. The green curve represents internal energy, whose trend clearly shows that nearly all kinetic energy is absorbed and converted into internal energy through plastic deformation and internal friction of the chassis structure. The cyan curve represents sliding energy, which remains extremely small and accounts for only a negligible proportion of the total energy, indicating that no abnormal or dominant frictional sliding occurs and that the simulation primarily reflects structural deformation. Overall, the smoothly increasing internal energy curve demonstrates that the collapse process of the front chassis structure is controlled and orderly. As kinetic energy decreases, internal energy increases, indicating energy exchange, and the decrease in kinetic energy is approximately equal to the increase in internal energy, confirming that the results are broadly consistent with the principles of energy conservation and conversion.

ISSN 2706-655X Vol. 8, Issue 2: 80-93, DOI: 10.25236/IJFET.2026.080211

### *5.5. Contact Force Analysis*

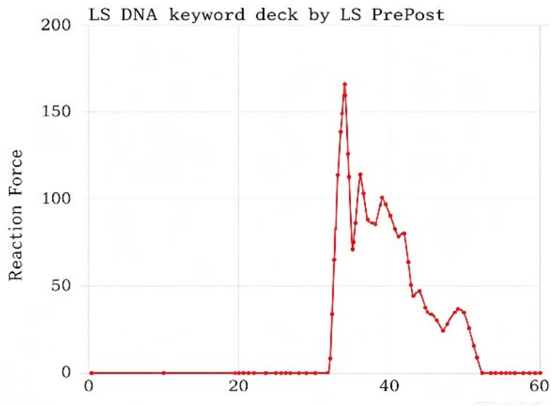


*Figure 10: Contact Force.*

Figure 10 shows that the maximum contact force during the initial collision reaches $1.68\times10^5$ N, indicating a severe impact between the front end of the chassis and the wall. As contact continues, the contact force gradually decreases, demonstrating that the chassis absorbs part of the impact energy through deformation. The front cross beams, longitudinal beams, and related structures successively undergo buckling and folding, producing several smaller force peaks and reducing the force directly transmitted to the vehicle body. As energy conversion proceeds, the contact force correspondingly decreases. After the first impact, the contact force peak becomes lower and the duration becomes longer, indicating better energy absorption and buffering performance in the subsequent response. The deformation region is mainly concentrated in the side-impact protection members and the two longitudinal and two transverse members of the front cabin. Based on the preceding results, the maximum deformation stress occurs at the intersection of the first and second cross beams, reaching 131 MPa, which is much lower than the yield strength of 4130 steel tubes and satisfies the required safety factor, indicating that this region is the primary zone for collision energy absorption.

### *5.6. Summary*

The simulation results indicate that the front diagonal braces and longitudinal beams play the primary buffering and energy-absorbing roles during collision, with deformation progressively propagating from front to rear while the main frame of the occupant cabin remains intact without collapse or fracture. The maximum stress occurs near the welded joints connecting the front cabin and the driver’s cabin, where the peak plastic strain reaches 0.342, close to the material failure threshold of 0.35, identifying this region as a structural weak point requiring subsequent reinforcement. The strain in the rear structure remains below 0.05 throughout the process, indicating good safety performance. Collision acceleration reaches its peak rapidly within approximately 8 ms, with the front bumper reaching 13 g, indicating a relatively severe impact; however, the subsequent curve is smooth, suggesting that the chassis retains additional energy absorption capacity. In terms of energy, kinetic energy is almost entirely converted into internal energy, while sliding energy accounts for only a small proportion, and total energy remains conserved, confirming the reliability of the simulation data. The contact force reaches a peak of approximately $1.68\times10^5$ N and then gradually decreases, with the front structure absorbing most of the impact through deformation. Overall, the chassis meets safety requirements and exhibits a reasonable energy absorption path, although two aspects still require improvement: the relatively high local strain at the front cabin connection and the steep collision acceleration pulse. These findings provide clear guidance for subsequent optimization.

## 6. Optimization and Improvement

### *6.1. Structural Optimization of the Model*

Since the simulation results indicate that the original chassis already exhibits relatively high safety performance, lightweight improvements were implemented, while weak regions were reinforced by increasing wall thickness or modifying the structural configuration to enhance stability, reliability, and safety.

ISSN 2706-655X Vol. 8, Issue 2: 80-93, DOI: 10.25236/IJFET.2026.080211

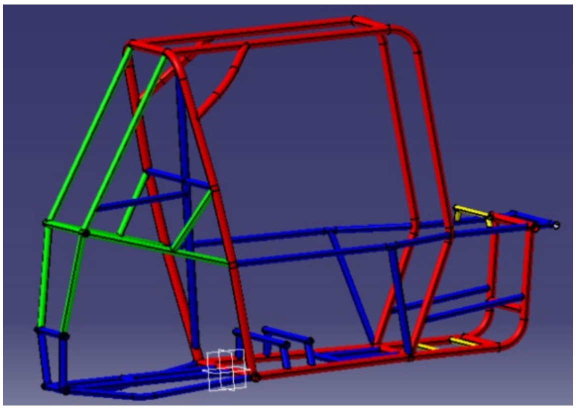

*Figure 11: Modified Chassis Model after Structural Optimization.*

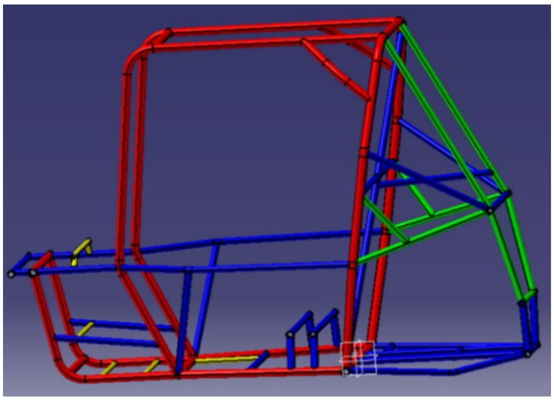

*Figure 12: Original Chassis Model before Structural Optimization.*

As shown in Figures 11 and 12, the chassis was modified in several aspects.

1) Because the rear cabin exhibited high safety performance, two blue diagonal members were removed; subsequent simulations demonstrated that the structure still maintained good energy absorption and safety performance.

2) The overall dimensions of the chassis were reduced, with the height decreased from 1250 mm to 1180 mm, the length from 1885 mm to 1850 mm, and the width from 760 mm to 700 mm.

3) The layout of the front cabin was adjusted to facilitate practical manufacturing.

4) The driver's cabin connection was changed from a single yellow vertical member to two blue members with larger outer diameter and greater wall thickness, thereby reducing the impact perceived by the driver and improving safety performance.

5) Unnecessary cross members in the front cabin were removed to reduce the overall vehicle mass.

### *6.2. Simulation Result Analysis*

To verify the effectiveness of the structural optimization scheme, collision simulations were conducted for the optimized chassis under the same operating conditions, and the results were compared with those of the original chassis, as shown in Figures 13–19 and Table 7.

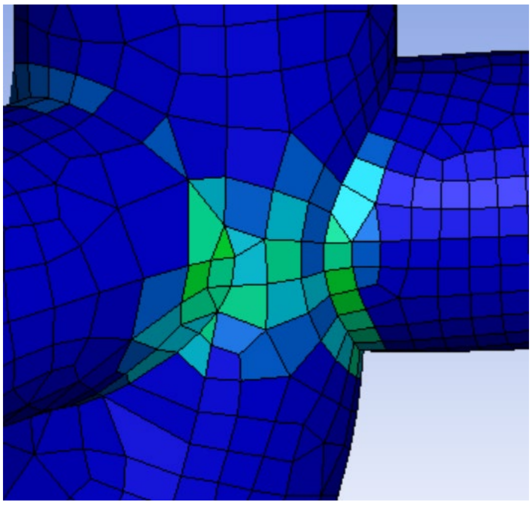

*Figure 13: Location of Maximum Strain after Optimization.*

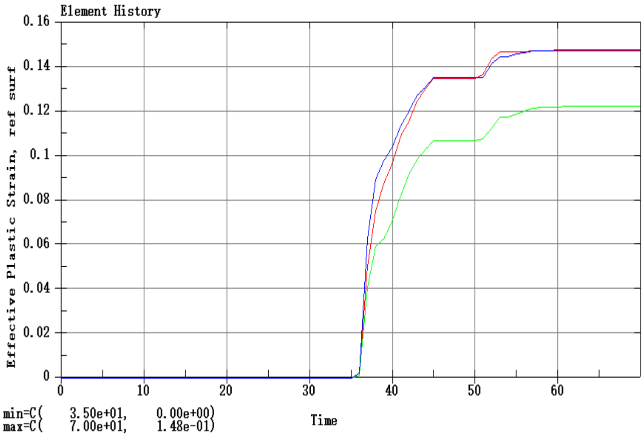


*Figure 14: Strain Contour Plot.*

From the perspective of stress–strain response, the maximum plastic strain of the optimized chassis decreases from 0.342 to 0.148, representing a reduction of 57%, which indicates that local plastic deformation during collision is significantly reduced. The strain contour plot shows that the high-strain region remains mainly concentrated at the connection between the front cabin and the driver's cabin; however, its distribution range is substantially narrowed and the peak value is reduced, demonstrating that the reinforcement measures in this region effectively suppress strain concentration and improve the structure's resistance to failure.

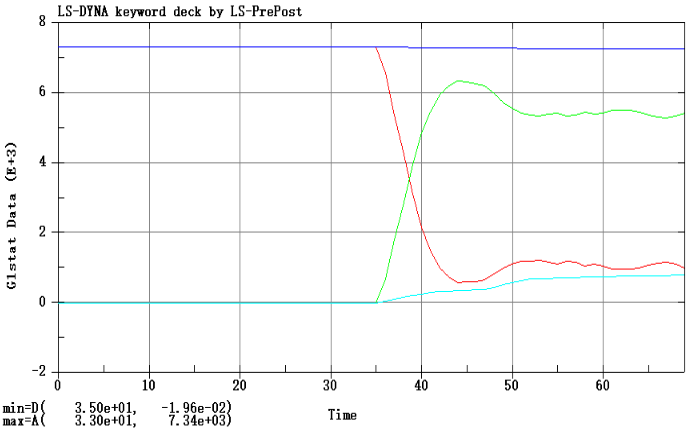


*Figure 15: Energy Curve.*

In terms of energy absorption characteristics, the internal energy trends before and after optimization are generally consistent, both showing rapid conversion of kinetic energy into internal energy while

ISSN 2706-655X Vol. 8, Issue 2: 80-93, DOI: 10.25236/IJFET.2026.080211

maintaining total energy conservation, indicating that the optimized structure does not alter the overall energy absorption mechanism. Meanwhile, the increase in internal energy becomes smoother, suggesting a more uniform structural deformation process that is beneficial for improving energy absorption efficiency.

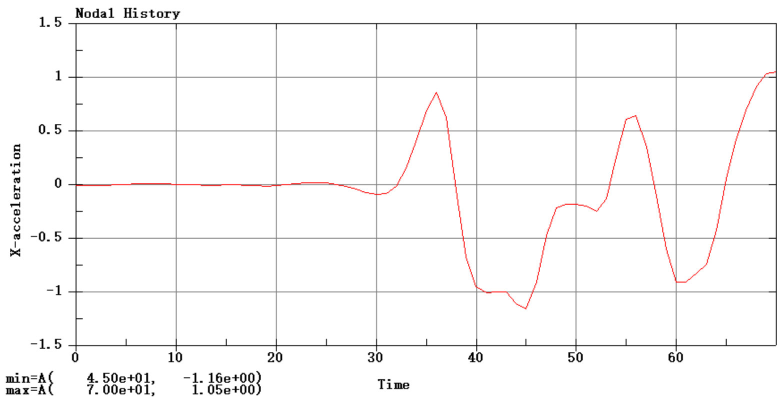


*Figure 16: Average Acceleration at the Front Seat Mounting Position on the optimized chassis.*

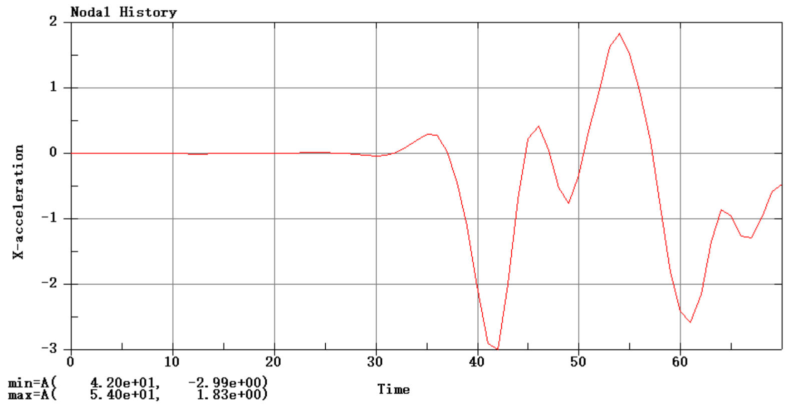


*Figure 17: Average Acceleration at the Rear Seat Mounting Position on the optimized chassis.*

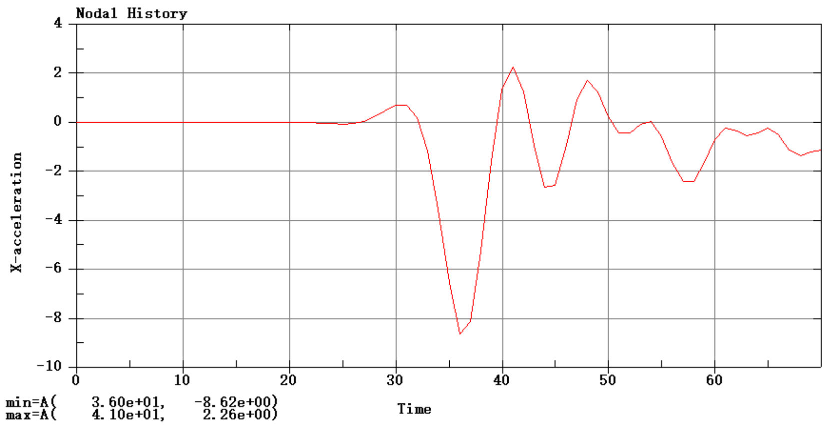


*Figure 18: Average Acceleration of the Front Bumper on the optimized chassis.*

From the perspective of dynamic response, the peak acceleration of the front bumper decreases from 13 g to 8.6 g, corresponding to a reduction of approximately 39%. The acceleration curves indicate that, after optimization, the rising rate of the impact pulse is reduced and the peak value decreases, suggesting that the front energy-absorbing structure can absorb impact energy more smoothly during the early collision stage, thereby reducing the impact load transmitted to the occupant cabin and improving occupant safety.

ISSN 2706-655X Vol. 8, Issue 2: 80-93, DOI: 10.25236/IJFET.2026.080211

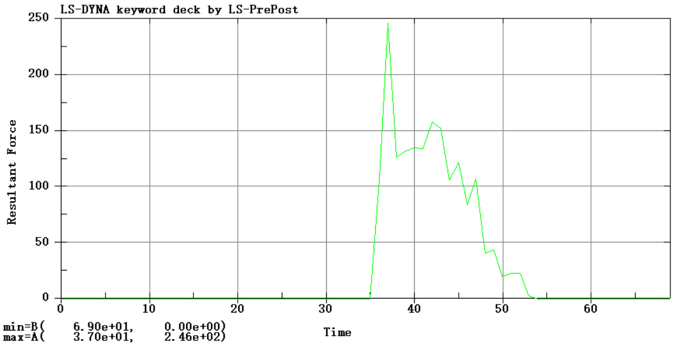


*Figure 19: Contact Force on the optimized chassis.*

Analysis of the contact force response shows that the peak contact force after optimization increases from $1.68\times10^5$ N to $2.46\times10^5$ N, representing an increase of approximately 46%. Although the peak value increases, the contact force curve exhibits a smoother variation trend, indicating that the structure carries the collision load through greater overall stiffness while still absorbing energy through structural deformation. Considering the strain and acceleration results together, the optimization scheme can be regarded as improving structural load-bearing capacity without worsening the impact response.

*Table 7: Comparison of Parameters before and after Optimization.*

| Indicator | Before Optimization | After Optimization | Rate of Change |
|---|---|---|---|
| Peak Plastic Strain | 0.342 | 0.148 | 57% |
| Peak Acceleration of Front Anti-Collision Beam | 13 g | 8.6 g | 39% |
| Peak Contact Force | $1.68\times10^5$ N | $2.46\times10^5$ N | 46% |

In summary, the optimized chassis demonstrates significant improvements in plastic strain control, acceleration response, and the energy absorption process, achieving coordinated optimization of lightweight design and safety performance and verifying the effectiveness of the proposed structural optimization scheme.

## 7. Conclusions

In this study, LS-DYNA was used to conduct frontal rigid-barrier collision simulations of a racing car space-frame chassis, and structural optimization was subsequently performed based on the simulation results. The main conclusions are as follows.

(1) Under the frontal collision condition at 11.11 m/s, the chassis exhibits typical progressive plastic collapse characteristics, with kinetic energy rapidly converted into structural internal energy within a short time. The energy absorption process is stable and consistent with the law of energy conservation. The front cabin longitudinal beams and diagonal braces serve as the primary energy-absorbing components, and collision deformation propagates gradually from the front of the chassis toward the rear, while the main structure of the occupant cabin remains intact and satisfies basic safety requirements.

(2) During the collision, stress and strain are mainly concentrated at the welded joints connecting the front cabin and the driver's cabin. The maximum equivalent stress is approximately 131 MPa, and the maximum plastic strain reaches 0.342, approaching the material failure threshold of 0.35, indicating that this region is a structural weak point. The strain in the rear structure remains consistently low, demonstrating good overall stiffness and safety.

(3) The collision dynamic response shows that the peak acceleration of the front crash structure is approximately 13 g, and although the impact pulse rises rapidly, the subsequent response remains stable, indicating that the structure possesses a certain degree of buffering and energy absorption capability. The maximum contact force is approximately $1.68\times10^5$ N and decreases as the structure progressively buckles and absorbs energy, demonstrating that the front structure can effectively attenuate the impact load.

(4) Based on the simulation results, targeted optimization was performed on the chassis structure, including local structural reinforcement and simplification of redundant members, thereby achieving lightweight design. After optimization, the chassis achieves reduced structural mass while improving stress concentration, acceleration response, and peak contact force, resulting in enhanced overall performance.

ISSN 2706-655X Vol. 8, Issue 2: 80-93, DOI: 10.25236/IJFET.2026.080211

(5) The “modeling–simulation–analysis–optimization” workflow established in this study can effectively identify critical weak regions during chassis collision and provide a basis for structural improvement, offering a useful reference for lightweight design and collision safety optimization of off-road racing car chassis.

## Acknowledgments

This work was supported by the 2025 Provincial Undergraduate Innovation and Entrepreneurship Training Program of Wuhan University of Technology (Grant No. S202510497116).

## References

*[1] Salanke S R S, Raju S S, Srinivas T S S N K, et al. (2025) A review on finite element modelling and experimental analysis of crashworthiness design of automotive body. International Journal of Crashworthiness, 30(5): 471-495.*
*[2] Chen H, Cui J T, Du Y F, et al. (2024) Topology Optimization Design of W-beams of Guardrails Based on LS-DYNA. 2024 4th International Conference on Digital Society and Intelligent Systems (DSINS), 438-442.*
*[3] Ren C, Yang X F, Liu X S. (2025) Crashworthiness evaluation of a BEV front-end system based on equivalent static crash stiffness method. Proceedings of the Institution of Mechanical Engineers, Part D: Journal of Automobile Engineering.*
*[4] Wang Z H, Sha Y Y, Jakobsen J B. (2024) Influence of local scour on the dynamic response of bridges under barge collisions. Engineering Structures, 308: 117941.*
*[5] Zhang H D, Qu Y, Wang K, et al. (2025) Numerical Study on the Dynamic Response of Composite Protective Covers Under Ship Anchor Impact. In: Proceedings of ASME 2025 44th International Conference on Ocean, Offshore and Arctic Engineering, OMAE2025, Vol 1.*
*[6] Xi X L, Liu X C, Bai C Y, et al. (2025) Full-scale impact test and high-fidelity numerical simulation of typical civil transport aircraft. Thin-Walled Structures, 212: 113147.*